Polymer 54 (2013) 4653–4659

Contents lists available at SciVerse ScienceDirect

Polymer

journal homepage: www.elsevier.com/locate/polymer

Higher-order crystalline structures of poly(oxyethylene) in poly(D,L-lactide)/poly(oxyethylene) blends

Nguyen-Dung Tien [a], Ta-Phuong Hoa [b], Masatsugu Mochizuki [c], Kenji Saijo [d], Hirokazu Hasegawa [d], Sono Sasaki [a,c], Shinichi Sakurai [a,c,*]

[a] Department of Biobased Materials Science, Kyoto Institute of Technology, Matsugasaki, Sakyo-ku, Kyoto 606-8585, Japan
[b] Polymer Centre, Hanoi University of Science and Technology, Viet Nam
[c] Center for Fiber and Textile Science, Kyoto Institute of Technology, Japan
[d] Department of Polymer Chemistry, Kyoto University, Japan

ARTICLE INFO

Article history:
Received 31 March 2013
Received in revised form
3 June 2013
Accepted 12 June 2013
Available online 20 June 2013

Keywords:
Higher-order crystalline structure
Poly(oxyethylene)
Poly(lactide)

ABSTRACT

Higher-order crystalline structures in blends of poly(lactide)/poly(oxyethylene) (PLA/PEG) were investigated using small-angle X-ray scattering (SAXS). For this purpose, the fact that two polymers are both crystalline makes situation much complicated. To simplify, we used non-crystalline PLA: poly(D,L-lactide) (DLPLA), which is a racemic copolymer comprising D- and L-lactide moieties. Higher-order peaks arising from the ordered lamellar stacking of PEG (i.e. the lattice peaks) were observed in the various blend samples, as well as in the PEG 100% sample, all of which were cast from their solutions in dichloromethane. Surprisingly, we found that the structure is more or less regular in the blend of DLPLA/PEG at compositions of 5–20 wt% of DLPLA than that in the PEG 100% sample. We further examined changes in such regular structures with temperature and found very peculiar SAXS profiles just 1 °C below melting temperature, which can be ascribed to a lamellar particle scattering. To our best knowledge, such a well-defined particle scattering has neither been reported for polymer blends, nor for the crystalline lamellar structure. Moreover, crossover from the lattice scattering to the particle scattering was observed in the temperature range from room temperature to 64 °C for the PEG 100% sample and blend samples with 5–20 wt% of DLPLA.

1. Introduction

Bio-based polymers have been attracting much attention recently due to the environmental issues. Among them, poly(lactic acid) (PLA) is one of the most promising materials because of its biodegradability and the fact that the monomer (lactide) can be efficiently obtained by fermentation from renewable resources such as cornstarch. Note also that by the ring-opening polymerization of lactide, it is possible to produce high molecular weight PLA. Since PLA has asymmetric carbons, we should care about two enantiomers, poly(L-lactide) (PLLA) and poly(D-lactide) (PDLA), which are both crystalline [1].

In spite of the prominent attraction of PLA, the application of PLA has been rather limited until now because of its relatively poor thermal stability [2], poor long-term durability [2,3] and also lower impact strength [3,4]. Among several approaches to improve the properties of PLA, blending of polymers is relatively simple and cost-effective. Miscibility, crystallization and properties of PLA blended with other polymers have been studied intensively [5–15]. Since poly(oxyethylene) (PEG) is known to be miscible with PLA in the amorphous phase, PEG has been utilized as a component to be blended with PLA. However, details of the higher-order structures of PEG crystallites in the blends with PLA have not yet been well understood. Therefore, we have just started structural analyses in the PEG/PLA blends [16] as an example of biodegradable polymer blends. For the study of the crystalline structure, the fact that two polymers are both crystalline makes situation much complicated. To simplify, we used non-crystalline PLA: poly(D,L-lactide) (DLPLA), which is racemic copolymer comprising D- and L-lactic acid moieties.

* Corresponding author. Department of Biobased Materials Science, Kyoto Institute of Technology, Matsugasaki, Sakyo-ku, Kyoto 606-8585, Japan. Tel.: +81 75 7247864.
E-mail address: shin@kit.ac.jp (S. Sakurai).

0032-3861
http://dx.doi.org/10.1016/j.polymer.2013.06.028

In this paper, we report results of the comprehensive studies on the higher-order crystalline structure of PEG in the DLPLA/PEG blends with various compositions and discuss the effects of DLPLA on the structure formation of PEG with thorough blend compositions. As reported in our previous rapid communication [16], we have found well-ordered meso-scale structure in the PEG 100% sample and the blends. This kind of regular structure is well known for the block copolymer as microphase-separated structure but of course quite unusual for the crystalline polymer or polymer blend. To analyze higher-order crystalline structure quantitatively, two-dimensional small-angle X-ray scattering (2d-SAXS) was utilized which can probe higher-order structures while wide-angle X-ray scattering (WAXS) that deals mainly with the primary crystalline structure (unit cell). Simultaneous measurements of SAXS and WAXS (SWAXS) [17] (namely, two position-sensitive area detectors are placed both for SAXS and WAXS set-up) covering wide angular range are powerful means to analyze structural changes on heating and/or cooling. Therefore, in our work, we have employed this 2d-SWAXS technique.

2. Experimental

DLPLA was purchased from Sigma–Aldrich Co. and used without further purification. Its weight-average molecular weight (M_w) is in the range of 75,000–120,000, the glass transition temperature $T_g = 44$ °C as revealed by DSC with the heating rate 10 °C/min (see Fig. 1(a)). PEG was purchased from Wako Pure Chemical Industries, Ltd. of which M_w = 20,000 and the melting point $T_m = 65.5$ °C as determined by DSC with the heating rate 10 °C/min (see Fig. 1(b)).

All blend samples were prepared by a solution-casting method. Given amounts of DLPLA and PEG were dissolved in dichloromethane yielding a solution with ca. 5 wt% polymer concentration. The solution was then poured into a flat Petri dish (φ 75 × 19 mm) for gradual evaporation of the solvent. An as-cast sample was obtained after complete evaporation of dichloromethane under ambient pressure at room temperature (~25 °C). Hereafter, the blend is referred to as DLx, where x represents the weight percentage of DLPLA in the blend.

The 2d-SWAXS measurements using the high brilliant synchrotron X-rays were carried out at BL-9C beamline with the wavelength of 0.150 nm, at BL-10C beamline with the wavelength of 0.1488 nm and at BL-15A with the wavelength of 0.150 nm, in Photon Factory of the High Energy Accelerator Research Organization, Tsukuba, Japan. An imaging plate (200 × 250 mm^2), of which actual pixel size is 100 × 100 μm^2, was used as a two-dimensional detector. The typical exposure time was in the range 30–100 s for SAXS and 10–30 s for WAXS, respectively. BAS2000 (Fuji Photo Film Co., Ltd.) was used for development of exposed images on the imaging plate. The 2d-SAXS patterns were obtained at BL-15A using either a charge-coupled device (CCD) camera with an image intensifier or an imaging plate as detectors; and at BL-10C using R-AXIS VII (Rigaku Denki Co., Ltd.). Collagen from a chicken tendon and polyethylene were used as standard samples for SAXS and WAXS, respectively, in order to calibrate the magnitude of the scattering vector, q, as defined by $q = (4\pi/\lambda)\sin(\theta/2)$ with λ and θ being the wavelength of X-ray and the scattering angle, respectively. The 2d-SAXS and 2d-WAXS patterns were further converted to one-dimensional profiles by conducting circular average or sector average occasionally.

3. Results and discussion

In Fig. 2, the change of the polymer concentration during the casting at room temperature was plotted. In the early stage, the evaporation of solvent took place linearly with time with the rate of 0.053 g/min. Around 2.78 g of solution weight (around 730 min elapsed), above which the solvent evaporation was retarded much where the polymer concentration was ca. 70 wt%, the casting solution became turbid, suggesting the onset of crystallization.

Let us discuss the SAXS results for the as-cast PEG 100% and various blend samples. Fig. 3 shows the one-dimensional SAXS (1d-SAXS) profiles measured at room temperature (around 28 °C). For the PEG 100% sample (DL0), higher-order peaks up to the seventh-order with the relative q positions of 1:2:3:4:5:6:7 are discernible. This suggests that stacking of crystalline lamellae of PEG is quite regular. From the position q^* of the first-order peak ($q^* = 0.262$ nm^{-1}), the lamellar repeating period (D) was evaluated as $D = 24.0$ nm through the Bragg's equation $D = 2\pi/q^*$. The fact that the successive orders up to seventh-order are discernable for the crystalline lamellar stack in the neat polymer is very striking if one can recognize that the general crystalline polymer such as polyethylene or polypropylene exhibits a single broad peak or sometimes up to second-order. This result clearly indicates that PEG can form a quite regular lamellar stacking structure which is comparably regular, similar to the block copolymer microdomain or even more than that. This further suggests that spontaneous regular folding of the polymer chains can be in a self-organized manner, which has been never expected before, although Shiomi et al. [18] have just published a similar SAXS profile without mentioning the significance.

Another significant finding here is that blending 20 wt% of DLPLA makes the lamellar stacks more regular as the 1d-SAXS profile exhibits sharper peaks as compared to the case of the PEG 100% sample and the other blends (DL5, DL10, DL50 and DL80). This kind of the favorable effects of blending has never been aware

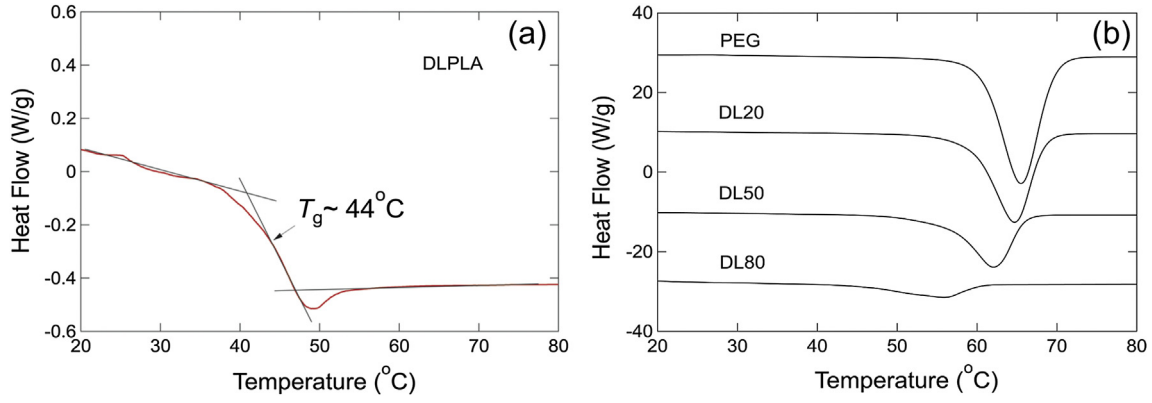

Fig. 1. DSC curves (heating rate: 10 °C/min) to determine (a) T_g of DLPLA and (b) T_m of PEG 100% and blend samples.

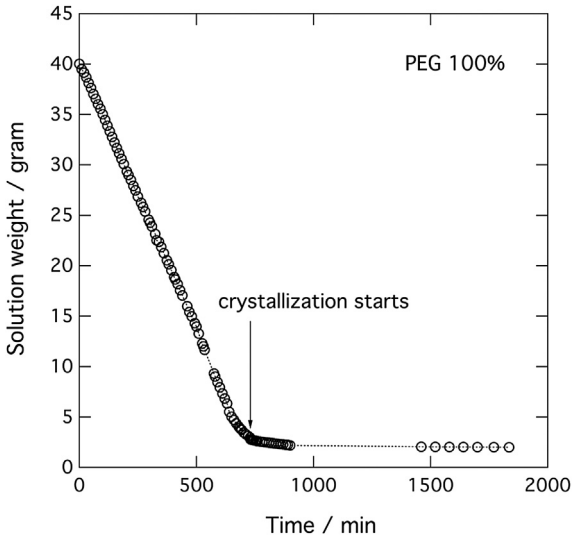

Fig. 2. Change in solution weight as a function of time during solution casting for the PEG 100% sample.

before, because it might be more or less reasonable to suppose that blending the other polymers makes the situation complicated and in turn spoil the regular structure. In order to show the change in the regularity quantitatively, we have applied the Hosemann's paracrystalline theory [19] and evaluated the distortion factor g which is given by $g = \Delta D/\overline{D}$ (where ΔD is the standard deviation of the lamellar repeating period). So-called Hosemann plot is shown in Fig. 4(a) where the peak width σ_q is plotted against n^2 for the n-th order reflection peaks. Here σ_q is the half width at the half maximum (HWHM). It can be seen that the data points firmly fall down onto a linear line (except DL10 and DL25). According to Hosemann, the reflection becomes broader when g-factor is larger (namely, the lattice regularity is lower), as

$$\sigma_q = \frac{1}{L} + 2\pi^2 g^2 n^2 \tag{1}$$

Note here that the grain size L can be also evaluated from the intercept. However, the evaluated value of L was extraordinary small. This may be due to the breadth owing to so-called collimation error of the SAXS camera. This error also affects the evaluation of the g-factor as it is under-estimated. And the degree of its under-estimation may be lower for the larger value of the g-factor. Therefore, change in the value of the g-factor as a function of the blend composition, as shown in Fig. 4(b), is not quantitative but qualitative. However, it is still possible to consider that the lamellar stacking is very much regular for DL20 since the evaluated value of g is smallest. Note here that the quite large error bar for the DL10 sample is ascribed to the wide distribution of the data points for this DL10 sample in Fig. 4(a). Revisiting the 1d-SAXS profile for this sample in Fig. 3 suggests that the 1st to 5th-order peaks are much broader than those for the other samples (DL0, DL5 and DL20), while the 6th and 7th-order peaks are not so broad, which are more likely sharper than those for the DL0 and the DL5 samples. Although we repeated SAXS measurement for the DL10 sample at least five times at the same condition, SAXS profiles were almost similar. To avoid mis-evalution of the g-factor from the Hosemann plot based on such an apparently broad peak, the factor of the peak broadening should be ruled out. The peak broadening may be due to the particle scattering, as is explained in more details later. In other words, the particle scattering should be separated out from the SAXS profile before the evaluation of the g-factor by the Hosemann plot. Another alternative way to evaluate the g-factor is through the parameter fitting to the experimentally obtained 1d-SAXS profile by conducting the model calculation with taking into account of both of the lattice and the particle scattering. Thus evaluated g values are more than twice of those evaluated from the Hosemann plot and under-estimation of the g-factor by Hosemann plot is clear, which in turn means that the reliability of the g-factor evaluated from the Hosemann plot is quite low. However, the tendency of the change in the g values (evaluated by the SAXS profile fitting) with the DLPLA content is found to be similar. Therefore, it can be concluded that the regularity of the higher-order structure is the best at DL20.

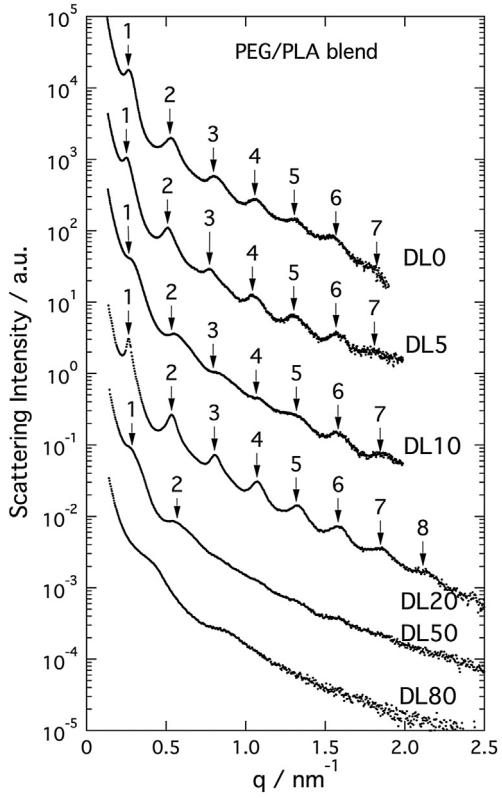

Fig. 3. 1d-SAXS profiles for the PEG 100% sample (DL0) and various DLPLA/PEG blend samples (DL5, DL10, DL20, DL50, DL80) with different compositions.

It is quite amazing to find that the higher-order structure is more regular in the DL20 blend sample as compared to the PEG 100% sample. One may suggest that the contrast between crystalline and amorphous phases would be larger for the DL20 sample than that for the PEG 100% sample and therefore much more higher-order peaks become discernable for the DL20 sample. To check whether this is the case or not, we calculate the electron density difference $\Delta\rho_e$ between the crystalline and amorphous phases. Considering that PEG chains are mixed with the DLPLA chains in the amorphous phase, $\Delta\rho_e$ should be express as follows

$$\Delta\rho_e = \left|\rho_e^{PEGc} - \langle\rho_e\rangle^a\right| \tag{2}$$

$$\text{with} \quad \langle\rho_e\rangle^a = \frac{(1-\varphi_{DLPLA}-x)\rho_e^{PEGa} + \varphi_{DLPLA}\rho_e^{DLPLA}}{1-x} \tag{3}$$

$$\text{and} \quad x = \bar{x}(1-\varphi_{DLPLA}) \tag{4}$$

where $\langle\rho_e\rangle^a$ and $\bar{x}$ represent the average electron density in the amorphous phase and normalized crystallinity of PEG in a blend sample (x is the bare crystallinity of PEG from the DSC results, see

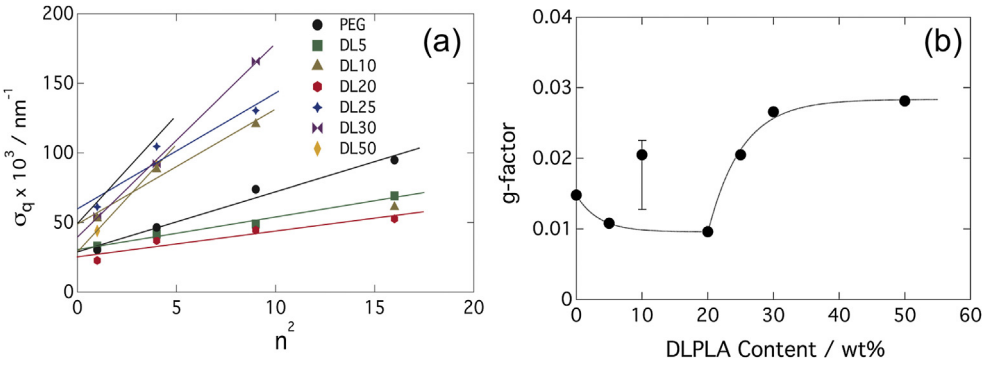

Fig. 4. (a) Hosemann plot and (b) plot of *g*-factor as a function of the DLPLA content.

Fig. 6), respectively. ρ_e^{PEGc}, ρ_e^{PEGa} and ρ_e^{DLPLA} represent the electron density of the crystalline PEG, amorphous PEG and DLPLA, respectively. To calculate them, each mass density is required. The literature values [20] of 1.235 (g/cm^3) for PEG crystal, 1.124 (g/cm^3) for PEG amorphous, and 1.248 (g/cm^3) for DLPLA are used for this purpose. $\rho_e^{PEGc} = 0.673$ (mole electrons/cm^3), $\rho_e^{PEGa} = 0.612$ (mole electrons/cm^3) and $\rho_e^{DLPLA} = 0.659$ (mole electrons/cm^3) are thus evaluated. Further evaluated values of $\Delta\rho_e$ for all blend samples are summarized in Table 1. It is found that $\Delta\rho_e$ decreases with an increase of the DLPLA content since the ρ_e^{DLPLA} is closer to ρ_e^{PEGc}. Therefore, the above-stated suspicious objection that the DL20 sample would have a larger electron density difference than the PEG 100% sample is then ruled out.

Another objection to the observation of more higher-order peaks for the DL20 sample comes from the difference in the detector length. Actually, the higher limit of the *q* range for the PEG 100% sample is less than that for the DL20 sample and therefore 8th-order peak would be observed even for the PEG 100% sample if the detector length would be sufficient. For this objection, it should be mentioned that the number of the lattice peaks discernible is not the issue in the Hosemann method, where the change in the peak sharpness with *n* is analyzed using that at most up to 4th-order. To conclude that the DL20 sample has a superior higher-order structure, we have conducted direct observation of the transmission electron microscopy (TEM). However, we found that TEM was not suitable to distinguish difference of the regularity among the blend samples and the PEG 100% sample, as well. The difference in the regularity we are discussing here, which can be analyzed by the SAXS method, is so small that such a localized structural analysis by the TEM method is out of accuracy. The reason why the blending 20 wt% of DLPLA made the PEG crystalline structure regular has yet been clearly understood, although this phenomenon is quite interesting. Note here that our separate SAXS experiments showed the lower lamellar regularity, thinner lamellae and shorter repeating period of the lamellar stacks both for the DL20 samples cast from the aqueous solution and non-isothermally crystallized from melts. These results indicate that the regular structure can be formed only from a dichloromethane solution. Therefore, the key may exist in the onset of crystallization from the solution during the solvent evaporation. Since PEG and DLPLA are miscible, PEG chains should sneak out from the homogeneous region of (PEG + DLPLA) mixture upon the onset of crystallization. Our results suggest that the presence of the DLPLA chains in the dichloromethane solution is convenient for PEG to conduct more regular chain folding which results in the smooth interface between amorphous and crystalline regions. Then, the degree of order of stacking becomes more regular because of the regular chain folding completed. Further investigation is required to check this mechanism.

As for the DL50 and DL80 blends, the regularity of the higher-order structure was much lower as compared to the PEG 100% because of too smaller amount of PEG. Actually for blend compositions below 20 wt% of DLPLA, peak positions almost do not change, indicating no big effect of blending on the lamellar repeating period as shown in Fig. 5. On the other hand for the DL50 sample, peaks become broader as compared to the PEG 100% sample and the peak position changes, which leads to the repeating period of 22.4 nm,

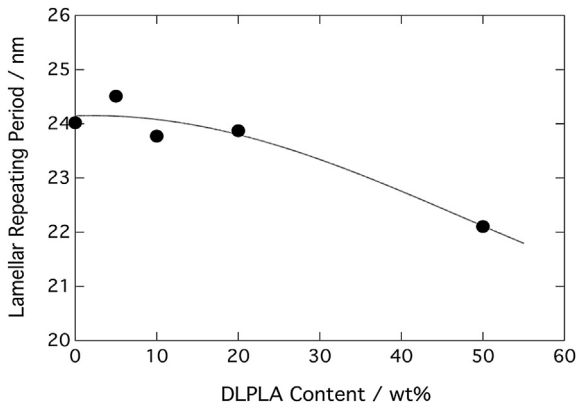

Fig. 5. Change in the lamellar repeating period with the DLPLA content.

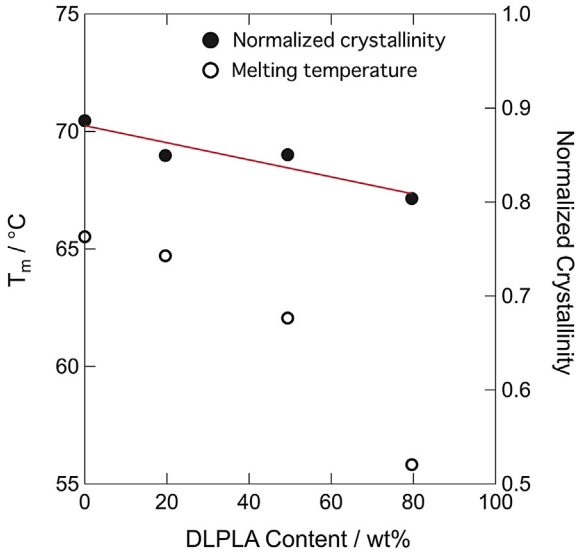

Fig. 6. Changes in the normalized degree of crystallinity and melting temperature as a function of the DLPLA content.

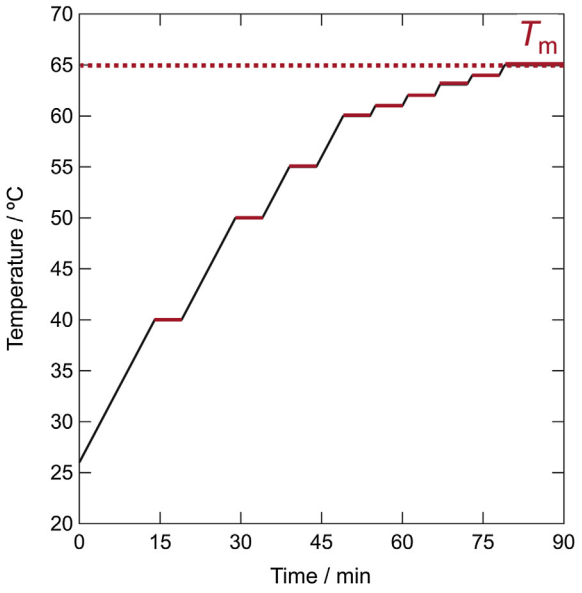

Fig. 7. Temperature protocol for the SWAXS measurement in the heating process.

Table 1
Electron density difference for the PEG 100% sample and blend samples.

Sample	$\bar{x}$	$\langle\rho_e\rangle^a$ (mole electrons/cm^3)	$\Delta\rho_e$ (mole electrons/cm^3)
DL0	0.88	0.612	0.061
DL20	0.85	0.641	0.032
DL50	0.85	0.653	0.020
DL80	0.80	0.657	0.016

6.7% reduction as compared to the PEG 100% sample. Although the similar tendency can be found for the DL80 sample, the 1d-SAXS profile including two broader peaks can be rather explained by the contribution of the particle scattering. This means that the crystalline lamellae exist sparsely in this blend sample without stacking. Since PEG and DLPLA are miscible, the PEG chains are homogeneously distributed in the cast solution just at the critical polymer concentration above which PEG starts crystallization. In the DL80 sample, only 20 wt% of PEG undergoes localized crystallization and therefore the stacking may not be allowed.

Based on the DSC results (Fig. 1), we determined the normalized crystallinity, $\bar{x}$, for the blend samples according to the following equation

$$\bar{x} = \frac{\Delta H_m}{\Delta H_m^o w_{PEG}} \times 100\% \quad (5)$$

where ΔH_m and ΔH_m^o are the enthalpy of fusion of the sample and the 100% crystal of PEG, respectively [20] and w_{PEG} is the weight fraction of PEG in the blend. The results are shown in Fig. 6. For the PEG 100% sample, the crystallinity is as high as ~0.90. Although the change in the normalized crystallinity is trivial, it is clearly observed that it decreases with an increase of the DLPLA content in the blend sample. This suggests lowering of the crystallizability of PEG due to its miscibility with DLPLA. As a matter of fact, melting point (T_m) depression is also observed in Fig. 6, as expected, although the decrease in T_m can be also explained as a consequence of the decrease in the lamellar thickness.

It might be considered that the structures formed in the as-cast sample is not at the thermodynamically equilibrium state because of vitrification of DLPLA of which glass transition temperature (T_g) is 44 °C (above temperature at which the solution cast was conducted i.e., room temperature). The structure is therefore subjected

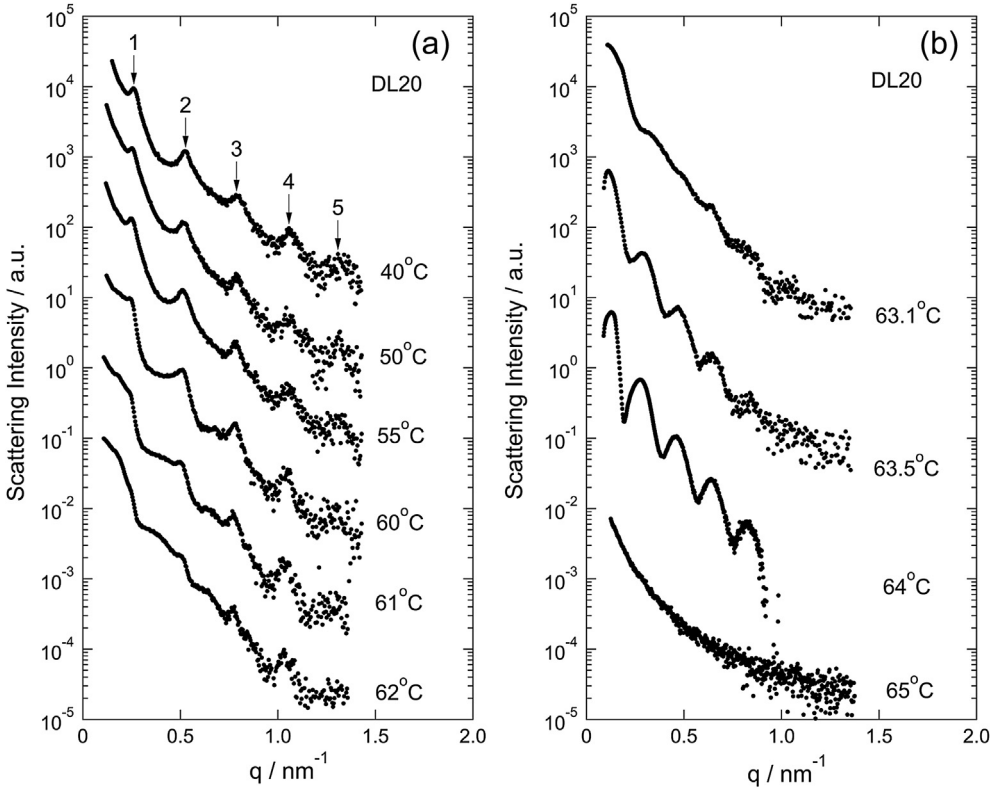

Fig. 8. Change in the 1d-SAXS profile with temperature (heating process) for the DL20 sample: (a) from 40 to 62 °C, (b) from 63.1 to 65 °C.

to change upon heating. To examine structural change upon heating, we conducted the in-situ SWAXS measurement for DL20 (see Figs. 8 and 9). The temperature protocol for the SWAXS measurement was presented in Fig. 7 where the red plateau portion indicates a duration for the isothermal SWAXS measurement at a given temperature. We focus here only on the DL20 sample because this sample showed very high regularity in the lamellar stacking. Many higher-order SAXS peaks were observed around 40–55 °C due to the regular stacking of the PEG crystallites. One can see the gradual change in the SAXS profile around 50–64 °C and then drastic change at 64 °C and 65 °C. Since 65 °C is above the melting temperature of PEG, crystalline lamellae are subjected to melting.

Therefore, no peaks are observed in the SAXS profile at 65 °C. The Lorentz-correction is required to rigorously check the existence of the SAXS peak, but there found to be no peak in the Lorentz-corrected SAXS profile [$q^2I(q)$ vs q]. A high intensity is, however, still observed in the SAXS profile at small q-range, suggesting that an unknown structure still exists even at 65 °C (above T_m).

It is noticeable that the SAXS profile measured at 64 °C which is only 1 °C below T_m exhibits peculiar shape, completely different from the ones measured in the temperature range from room temperature to 55 °C in the heating process. Although the profile shows many peaks, the relative q positions cannot be expressed by the simple digits (1:2:3…) which indicates clearly that those peaks are not the lattice peaks. Here, we should remind that the scattering comprises not only the lattice factor (due to the interparticle interference) but also the particle scattering (due to the intra-particle interference). Since the peaks do not seem to be due to the lattice factor, the profile at 64 °C may be due to the particle scattering. In order to explain the change in the SAXS profile with temperature, we conduct the model calculation of the SAXS profile for the one-dimensionally repeating lamellae (1d-lattice), by just following full equations presented by Shibayama and Hashimoto [21]. $I(q)$ is given as

$$I(q) = q^{-2}\left[\left\langle f^2\right\rangle - \langle f\rangle^2 + \langle f\rangle^2\left\{Z(q) + I_c/N\right\}\right] \tag{6}$$

for the randomly-oriented 1d-lattice system, where I_c is the zeroth-order scattering intensity (see Ref. [21] for details), N is the number of stacked lamellae in a grain, f and $Z(q)$ are the particle scattering and the lattice factor, respectively, where

$$\langle f\rangle = \sum_L n(L)L\left\{\frac{\sin(qL/2)}{qL/2}\exp\left(-\sigma^2q^2/2\right)\right\} \tag{7}$$

$$\left\langle f^2\right\rangle = \sum_L n(L)L^2\left\{\frac{\sin(qL/2)}{qL/2}\exp\left(-\sigma^2q^2/2\right)\right\}^2 \tag{8}$$

where $n(L)$ is the number fraction of lamella of which thickness is L existing in the sample and σ characterizes interfacial thickness.

$$Z(q) = \frac{1-|F|^2}{1-2|F|\cos(qD)+|F|^2} \tag{9}$$

with

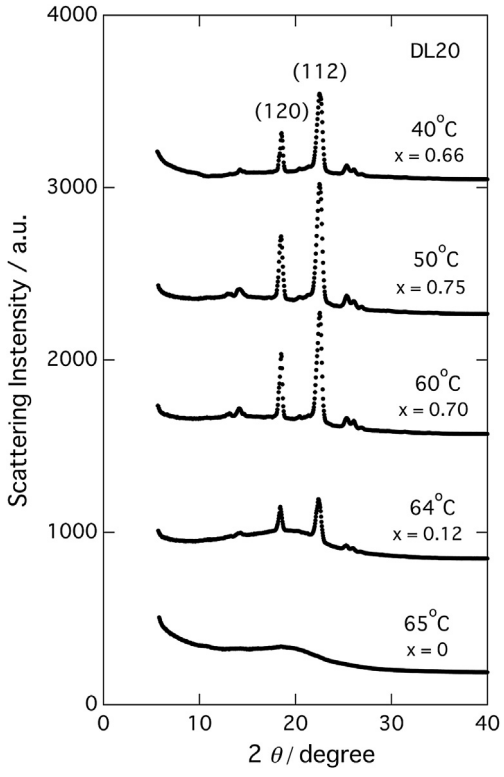

Fig. 9. Change in the 1d-WAXS profile with temperature (heating process) for the DL20 sample. Here, x denotes the bare crystallinity evaluated by using the area for the crystalline and the amorphous peaks after peak decomposition. It is also noted that the θ axis is rescaled to enable us to directly compare the profile with that measured using conventional SAXS apparatus with CuK$_\alpha$ radiation (λ = 0.154 nm). Therefore, the θ value is converted from the q value using $\lambda = 0.154$ nm, although we used $\lambda = 0.150$ nm in the real measurement.

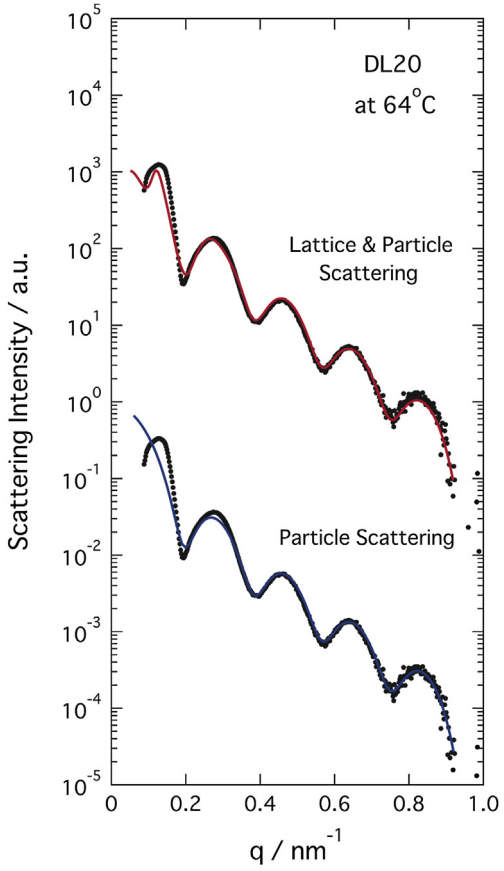

Fig. 10. 1d-SAXS profile for DL20 at 64 °C and the best–fit profile (solid red curve) for the full calculation including the lattice factor and the particle scattering. The blue curve shows the particle scattering. (For interpretation of the references to color in this figure legend, the reader is referred to the web version of this article.)

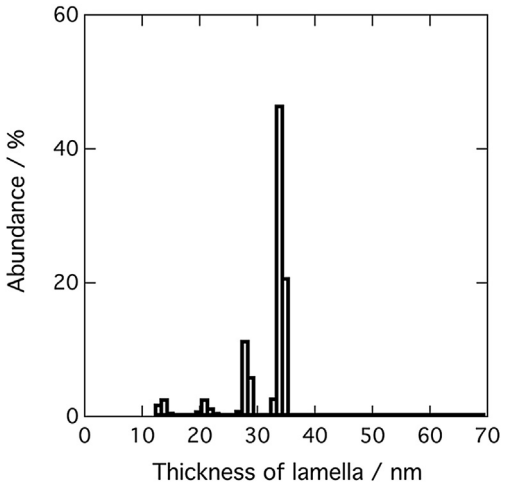

Fig. 11. Distribution of lamellar thickness used for the calculation of the particle scattering.

$$|F| = exp\left(-g^2D^2q^2/2\right) \quad (10)$$

In order to clearly show that the characteristic feature of the SAXS profile observed at 64 °C is ascribed to the particle scattering, $\langle f(q)^2\rangle$ is separated out from the best–fit profile (shown in red in Fig. 10) and compared with the experimentally measured SAXS profile in Fig. 10 shown with a blue solid curve and the black filled circles, respectively. Note that $\langle f(q)^2\rangle$ is calculated with the distribution of L shown in Fig. 11. One can see all of the peaks (excepting for the first-order peak) can be explained by the particle scattering, so that we can conclude that there are isolated crystalline lamellae of PEG dispersed in the amorphous matrix at 64 °C.

Although the SAXS result reminds that almost-isolated lamellar particles are randomly dispersed in the amorphous matrix, it is required to consider that lamellae form a stack with the repeating period $D = 48.0$ nm, as determined by the SAXS fitting (also evaluated from the position of the first-order peak). The ratio of L and D gives crystallinity for the one-dimensionally repeating system. For the particular case at 64 °C, $L = 33.5$ nm (see Fig. 11) and $D = 48.0$ nm give $L/D \approx 0.70$, which is extraordinary larger than the bare crystallinity 0.12 evaluated from the WAXS result (Fig. 9). In order to satisfy the quite low degree of crystallinity, the model illustrated in Fig. 12 bearing the large amount of the amorphous matrix is considered.

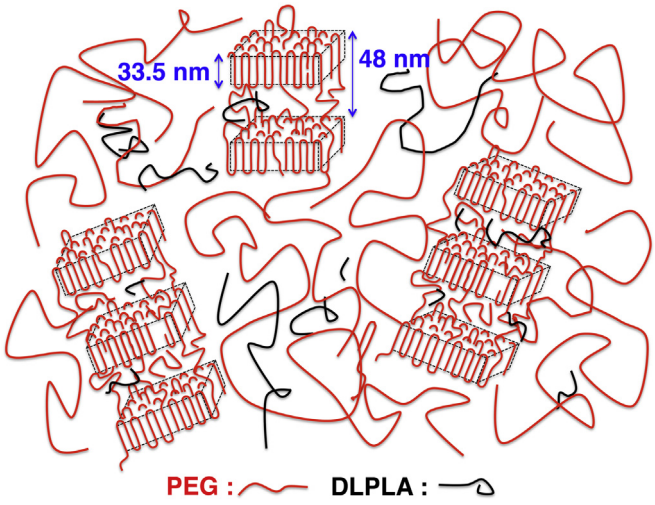

Fig. 12. Possible model of the DL20 blend sample at 64 °C.

4. Conclusions

In this study, blend samples of non-crystalline DLPLA and PEG were subjected to structural analyses to examine effects of blending DLPLA (biobased materials) on the higher-order crystalline structures of PEG. The structure is found to be more regular for the DL20 sample than for the PEG 100% sample. The better regularity in the DL20 sample was confirmed by several methods to analyze the SAXS profile showing lattice peaks up to 8th-order one. Furthermore, very peculiar SAXS profile was observed at 64 °C, just only 1 °C below T_m of PEG, for the DL20 sample. This is found to be a particle scattering of lamellae, which has neither been reported for polymer blends, nor for the crystalline polymer. Based on the results, we proposed a plausible model that a couple of lamellar particles are stacked and this stack is randomly dispersed in the amorphous matrix. The reason why the blending 20 wt% of DLPLA made the PEG crystalline structure regular has yet been clearly understood, although this phenomenon is quite interesting. Since PEG is widely utilized for many applications, the superior ability of DLPLA to upgrade PEG is promising for the future developments of new functional materials.

Acknowledgments

We are deeply grateful to Prof. Nishikawa at Kyoto Institute of Technology and Prof. Tosaka at Kyoto University for their fruitful discussion. We also thank technical support for the SAXS experiments from Dr. Shimizu at KEK, Dr. Masunaga at SPring-8 and Mr. Kimura in Kyoto Institute of Technology. The SAXS experiments were performed at BL40B2 (JASRI) and BL03XU (Advanced soft-material BL consortium) in SPring-8, Japan (approval number 2010A3306, 2010A7225, 2010B1110, 2010B3306, 2010B7271, 2011B3306, and 2012A3306), and at KEK-PF with the approval number 2011G613. We are deeply indebted to the Nitto Denko Corporation and the Asahi-Kasei Corporation for their partnerships upon conducting the experiments using the Advanced softmaterial BL consortium.

References

[1] Siparsky G, Voorhees K, Dorgan J, Schilling K. Journal of Polymers and the Environment 1997;5(3):125–36.
[2] Fukushima K, Hirata M, Kimura Y. Macromolecules 2007;40(9):3049–55.
[3] Meaurio E, Zuza E, Sarasua J-R. Macromolecules 2005;38(4):1207–15.
[4] Hualin W, Yan Z, Min T, Linfeng Z, Zheng W, Tiejun S. Journal of Applied Polymer Science 2008;110(6):3985–9.
[5] Nakafuku C. Polymer Journal 1996;28(7):568–75.
[6] Nakafuku C, Sakoda M. Polymer Journal 1993;25(9):909–17.
[7] Nijenhuis AJ, Colstee E, Grijpma DW, Pennings AJ. Polymer 1996;37(26):5849–57.
[8] Tsuji H, Fukui I. Polymer 2003;44(10):2891–6.
[9] Tsuji H, Hyon SH, Ikada Y. Macromolecules 1991;24(20):5651–6.
[10] Tsuji H, Hyon SH, Ikada Y. Macromolecules 1991;24(20):5657–62.
[11] Tsuji H, Ikada Y. Polymer 1996;37(4):595–602.
[12] Tsuji H, Ikada Y. Journal of Applied Polymer Science 1996;60(13):2367–75.
[13] Tsuji H, Ikada Y. Journal of Applied Polymer Science 1997;63(7):855–63.
[14] Yang J-M, Chen H-L, You J-W, Hwang JC. Polymer Journal 1997;29(8):657–62.
[15] Younes H, Cohn D. European Polymer Journal 1988;24(8):765–73.
[16] Tien ND, Hoa TP, Kimura G, Yamashiro Y, Fujiwara H, Mochizuki M, et al. Journal of Physics: Conference Series 2011;272(1):012007.
[17] Chu B, Hsiao BS. Chemical Reviews 2001;101(6):1727–62.
[18] Shiomi T, Takeshita H, Kawaguchi H, Nagai M, Takenaka K, Miya M. Macromolecules 2002;35(21):8056–65.
[19] Hosemann R, Bagchi SN. Direct analysis of diffraction by matter. Amsterdam: North-Holland 1962.
[20] Brandrup J, Immergut EH. Polymer handbook. 3rd ed. New York: Wiley-Interscience; 1989.
[21] Shibayama M, Hashimoto T. Macromolecules 1986;19(3):740–9.